Preprints of the 19th World Congress
The International Federation of Automatic Control
Cape Town, South Africa. August 24-29, 2014

Loss Minimization and Voltage Control in Smart Distribution Grid

Morten Juelsgaard [*], **Christoffer Sloth** [*], **Rafael Wisniewski** [*] **and Jayakrishnan Pillai** [**]

[*] *Automation and Control, Aalborg University, Fredrik Bajers Vej 7C, 9220 Aalborg Øst, Denmark, contact {mju,ces,raf}@es.aau.dk*
[**] *Energy Technology, Aalborg University, Pontoppidanstræde 101, 9220 Aalborg Øst, Denmark, contact jrp@et.aau.dk*

Abstract: This work presents a strategy for increasing the installation of electric vehicles and solar panels in low-voltage grids, while obeying voltage variation constraints. Our approach employs minimization of active power losses for coordinating consumption and generation of power, as well as reactive power control to maintain satisfactory grid operation. Numerical case studies illustrate how our approach can significantly increase installation of both electric vehicles and solar panels, while avoiding unsatisfactory over- and under-voltages throughout the grid.

Keywords: Energy distribution, loss minimization, voltage stability, energy management

1. INTRODUCTION

The low-voltage distribution grid faces increasingly significant challenges, compared to the traditional operation of the grid. These challenges emerge from an increasing load in the grid, as well as increasing levels of power production at household level.

The increased load is caused by an enhanced use of electricity for instance for transportation or heating, *i.e.*, energy consumption that has previously been accommodated by fossil fuels, as forecasted by the Danish Energy Association and Energinet.dk (2010), as well as the International Energy Agency (2011). The challenges emerging from this lies in the risk of overloading the distribution grid, as well as increased distribution grid losses, and increased risk of unsatisfactory power quality. Specifically, the current lack of charging rules or guidelines for electric vehicles (EVs), entails that the low-voltage distribution grid is currently not suited for large scale implementation of these, due to the risk of grid-overload and unacceptable voltage drops, as shown by Pillai et al. (2012).

The increased penetration of household power production stems from installations of solar panels, household wind turbines, *etc.* Introducing significant levels of local power production, may challenge the unidirectional power flow paradigm, under which the grid has been designed. If the power produced locally is not also consumed locally, the power will not flow exclusively from the grid towards the consumers. Rather, power will also flow in the converse direction. This carries the risk of over-voltages occurring throughout the grid.

The combined effect of increased load, and local production, can be illustrated with the following abstract example: Imagine a low-voltage distribution grid, connected to the medium voltage grid through a step-down transformer. The grid is designed with a line topology, that is a single feeder, without branches. The grid contains 50 consumers, where the 18 consumers closest to the transformer (indexed $1-18$), each have an EV installed, and the 14 consumers furthest from the transformer (indexed $36-50$) each have a photo-voltaic (PV) array installed.

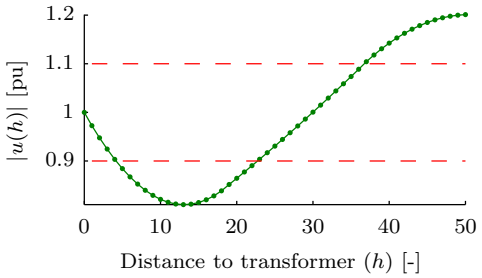

Fig. 1. Voltage in the connection point h, of each consumer throughout the feeder (dots), and allowed voltage variation (dashed).

Fig. 1 shows the voltage profile of the feeder at one fixed time instance where all EVs are charging, while all solar panels produce power. As illustrated in Fig. 1, the charging of vehicles causes an unacceptable voltage drop in the initial part of the radial, where the EVs are connected. Meanwhile, all PV owners produce excess solar power, which is not consumed locally, resulting in a local voltage increase in the furthest part of the feeder, violating the maximum voltage limit. Thus, there is both massive over- and under-voltages at the same time throughout the feeder. In this work, we present an implementation strategy on how these issues may be reduced through optimization and coordination.

Traditional measures for maintaining stable voltages in low-voltage (LV) grids, are based on an assumption of uni-directional power flow, such that the voltage will drop along the feeder. As bi-directional power flows become increasingly common, this will not pertain to be the case,

requiring revisions of the traditional control strategies as discussed by Ipakchi and Albuyeh (2009). Specifically, in the example presented above, standard voltage control strategies, such as transformer tap-changers for voltage control, might very well raise the voltage to an acceptable level in the initial part of the feeder; however, it would conversely worsen the over-voltage issue at the end of the feeder.

This paper is a continuation of the work by Juelsgaard et al. (2013), where it was illustrated how control of EV power consumption could be employed for coordination, in order to minimize the incurred power loss, and reduce the overall grid loading. In the work at hand, we expand on this idea, and show how loss minimization can be used for coordinating consumption by EVs against production from solar panels, in order to increase the possible installation of both, without unacceptable voltage variations. We further include reactive power control of solar panel inverters, and illustrate both the potential and limits of its effect on voltage stabilization.

Active control of consumers, with the purpose of avoiding voltage variations and grid overload has been considered by *e.g.*, Pillai et al. (2012), who presented a heuristic control strategy for charging a fleet of EVs. Consumer control was similarly investigated by Turitsyn et al. (2011), who discussed the design of local control of reactive power from solar panel inverters, with the purpose of reducing voltage variation and power losses. Compared to these works, we consider the installation of EVs and PVs collectively in the grid, rather than separately, and illustrate how they may be coordinated to alleviate the above issues. Also, we are not concerned with voltage variations specifically, rather we are concerned with obeying variational limits, while minimizing losses.

Loss minimization was also the main focus of Baran and Wu (1989), who considered grid reconfiguration for loss reduction, and Hoff and Shugar (1995); Guo et al. (2011), who investigated where to locate distributed generation, such as PVs, in the LV grid, in order to reduce losses. Compared to these works, this paper does not attempt to modify the grid or pick beneficial PV installation locations. Rather, we introduce a coordination strategy which can be employed for loss reduction and voltage control, in a predefined grid layout and PV installation.

The remainder of this paper is organized as follows: Section 2 outlines our modeling approach, and presents the formal problem description. Section 3 addresses our approach towards solving the coordination problem, and describes a benchmark strategy for result comparison. A practical test-case, used for numerical experiments, is presented in Section 4, followed by examples in Section 5. Concluding remarks are presented in Section 6.

2. MODELING AND PROBLEM FORMULATION

In this section, we model the consumers in the LV grid, as well as the distribution lines feeding them with electricity. Subsequently, we describe the optimization problem of minimizing active power losses by coordinating consumers.

2.1 Consumer modeling

A household is modeled as a potential prosumer (combined producer and consumer), with active and reactive power given by

$$p_h(t) = \overline{p}_h(t) + \tilde{p}_h(t), \quad \text{and} \quad q_h(t) = \overline{q}_h(t) + \tilde{q}_h(t),$$

for each household $h \in \mathcal{H} = \{1, \dots, n\}$ and time step $t \in \mathcal{T} = \{1, \dots, T\}$. Above, $\overline{p}_h$ and $\overline{q}_h$ refer to the part of the power that is inflexible, that is, it cannot be controlled or temporally shifted. Contrary, $\tilde{p}_h$ and $\tilde{q}_h$ represent power that allows for a certain degree of flexibility. In this work, the flexibility originates from the charging of EVs and reactive power control of PVs. Throughout, we consider only average active and reactive power over some time period; not instantaneous power. This entails that the time dependency included in the notation, refers to the average power consumption throughout period $t \in \mathcal{T}$ with fixed time period T_s.

We denote by $\mathcal{H}_{\text{ev}} \subseteq \mathcal{H}$ the households with EVs. The power used for charging each vehicle $h \in \mathcal{H}_{\text{ev}}$ represents flexible consumption at a constant power factor ψ_h. For each vehicle, $t_{\text{ev},h}$ denotes the time the electric vehicle is plugged in. The energy in the EV battery, *i.e.*, the state of charge (SOC), then follows the charge pattern

$$E_{\text{ev},h}(t) = E_{\text{ev},h}(t_{\text{ev},h}) + \sum_{\tau=t_{\text{ev},h}}^{t} T_s \tilde{p}_{\text{ev},i}(\tau), \quad \forall h \in \mathcal{H}_{\text{ev}},$$

where $E_{\text{ev},h}(t_{\text{ev},h})$ denotes the charge when the vehicle is plugged in and $\tilde{p}_{\text{ev},h}(\tau)$ is the average active power consumption of the vehicle during period $\tau \in \mathcal{T}$.

The power consumption, $\tilde{p}_{\text{ev},h}(t)$, of each EV is controllable, but is limited by the following constraints

$$E_{\text{ev},h}(T) = E_{\text{dem},h}, \quad E_{\min,h} \le E_{\text{ev},h}(t) \le E_{\max,h},$$
$$p_{\min,h} \le \tilde{p}_{\text{ev},h}(t) \le p_{\max,h},$$
$$\tilde{q}_{\text{ev},h}(t) = \tilde{p}_{\text{ev},h}(t) \tan(\operatorname{acos}(\psi_h)),$$

for all $t \in \mathcal{T}$ and $h \in \mathcal{H}_{\text{ev}}$. Above, $\tilde{q}_{\text{ev},h}(t)$ is the reactive power consumed by the EV in time period t, $E_{\min,h}$, $E_{\max,h}$ and $E_{\text{dem},h}$ denote minimum, maximum and required final SOC, respectively. Similarly, $p_{\min,h}$ and $p_{\max,h}$ are minimum and maximum EV power limits.

In this work, we introduce residential power production through photovoltaic solar panels. We denote by $\mathcal{H}_{\text{pv}} \subseteq \mathcal{H}$ the households with PV installed. These produce active power $\overline{p}_{\text{pv},h}(t) \ge 0$, and reactive power $\tilde{q}_{\text{pv},h}(t)$, $h \in \mathcal{H}_{\text{pv}}$. The active power is uncontrollable and determined from weather conditions, *i.e.*, direct/indirect radiation, clouds, *etc.* On the other hand, the reactive power is controllable, with the constraint

$$|\tilde{q}_{\text{pv},h}(t)| \le \sqrt{s^2_{\max,h} - \overline{p}^2_{\text{pv},h}(t)}, \quad \forall t \in \mathcal{T} \tag{1}$$

where $s_{\max,h} > 0$ is a fixed upper limit of apparent power for the solar panel inverter. This constraint is similar to the work by Turitsyn et al. (2011), and is essentially a constraint on the maximum magnitude of the inverter current.

The inverter technology allowing reactive power control of PVs exists also in the EV inverters, whereby reactive power control of the EVs could equally well be introduced in this work. We shall, however, limit our investigation to

PV reactive power control, and leave the similar study of EVs for later work.

Given the modeling above, the total active and reactive power consumption of a consumer is then

$$p_h(t) = \overline{p}_h(t) + \tilde{p}_{\mathrm{ev},h}(t) - \overline{p}_{\mathrm{pv},h}(t),$$
$$q_h(t) = \overline{q}_h(t) + \tilde{q}_{\mathrm{ev},h}(t) - \tilde{q}_{\mathrm{pv},h}(t).$$

We remind the reader that consumers at any time may produce rather than consumer active and reactive power. This entails that the above is to be understood as consumption if $p_h(t) > 0$ and production when $p_h(t) < 0$ and similarly for $q_h(t)$.

Throughout the remainder of the paper, we let it be implied that $\overline{p}_{\mathrm{pv},h}, \tilde{q}_{\mathrm{pv},h} \equiv 0$ for $h \notin \mathcal{H}_{\mathrm{pv}}$, and $\tilde{p}_{\mathrm{ev},h}, \tilde{q}_{\mathrm{ev},h} \equiv 0$ for $h \notin \mathcal{H}_{\mathrm{ev}}$.

2.2 Grid modeling

The low-voltage (LV) (0.4 kV) grid consists of the distribution cables feeding power to each consumer.

The LV grid is connected to the medium voltage grid, through a transformer. For simplicity, the medium voltage grid and transformer station are abstracted by an ideal voltage source, i.e., the secondary side voltage of the transformer $u_{\mathrm{s}} \in \mathbf{R}$, has zero phase and constant magnitude and frequency. In addition, we assume that the grid is balanced, allowing the analysis to be performed for an equivalent single phase system, see Kundur (1993).

The distribution lines are modeled as approximate π-circuits, where the shunt capacitances are neglected, since the cables in the considered grid are short. Thus, distribution lines are modeled as RL-series impedances. Let $m \in \mathbf{N}$ be the number of cable sections in the considered grid. The value of the impedance for each grid section is denoted $z_k = r_k + \mathrm{j}\omega L_k \in \mathbf{C}$ for all $k \in \{1, \ldots, m\}$, where r_k, L_k and ω denote resistance and inductance of each cable, and grid frequency, respectively.

Given the notational convention introduced so far, the grid and associated residents are illustrated conceptually in Fig. 2.

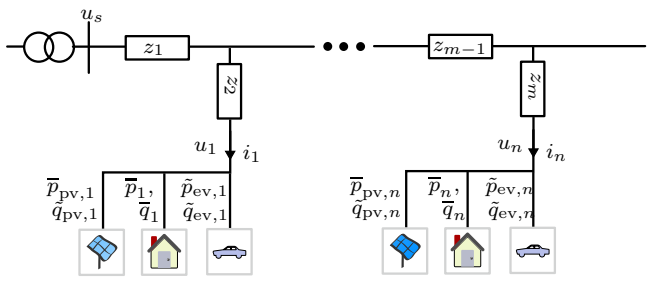

Fig. 2. Conceptual outline of a radial of the low-voltage grid, illustrating the consumers, with active and reactive solar production $(\overline{p}_{\mathrm{pv}}, \tilde{q}_{\mathrm{pv}})$, EV consumption $(\tilde{p}_{\mathrm{ev}}, \tilde{q}_{\mathrm{ev}})$, and inflexible consumption $(\overline{p}, \overline{q})$.

2.3 Grid losses

The root-mean-square (RMS) phasor-voltage in the connection point of consumer h, is denoted $u_h(t) \in \mathbf{C}$. The corresponding RMS phasor-current $i_h(t) \in \mathbf{C}$, drawn by the consumer is

$$i_h(t) = f(p_h(t), q_h(t), u_h(t)) = \left(\frac{p_h(t) + \mathrm{j}q_h(t)}{u_h(t)}\right)^{\dagger}, \quad \forall t \in \mathcal{T}, \quad (2)$$

where the functional f is introduced to ease notation onwards, and $\dagger$ denotes conjugate transpose. From the current of each consumer, we can derive an expression for the power losses throughout the grid. We remark that the distribution grid can be visualized as a graph, where each cable represents an edge. Following the convention of Desoer and Kuh (2010), the graph can be decomposed as a spanning tree, whose edges are called branches, and the remaining set of edges are called links. In practice, the branches would be the cables composing each feeder of the grid, whereas links would be closed switches, creating paths between each feeder as illustrated in Fig. 3(Left).

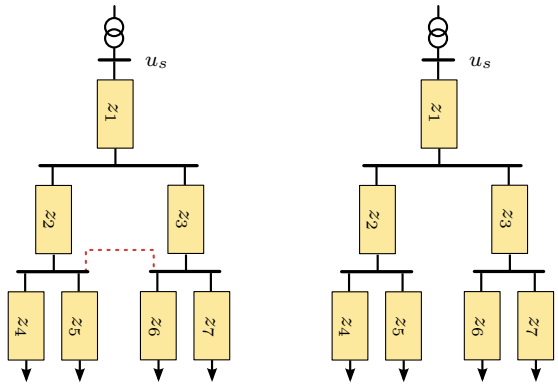

Fig. 3. **Left:** Graph structure of a small grid example. The arrows represent consumers. Each consumer and busbar in the grid is a node in the graph, and each cable-impedance is an edge. The dashed line illustrates a link, representing a closed switch between two feeders. **Right:** A similar grid, without links.

For the sake of clarity, this work focuses on distribution grids without links, *i.e.*, their underlying topology is a tree, similar to the grid illustrated in Fig. 3(Right). Our work generalizes to any connected grid topology, but the matrices to be introduced shortly are then highly dependent on the topology of the specific network.

Conforming to the taxonomy of Desoer and Kuh (2010), we let the transformer substation denote the root node of the tree, and the consumers denote leaf nodes. For each $h \in \mathcal{H}$, let $\mathcal{Z}_h \subseteq \{1, \ldots, m\}$ denote the set of impedance indices of the unique simple path between the transformer and consumer h. We define $J = [J_{x,y}] \in \mathbf{C}^{n \times n}$ as

$$J_{x,y} = \sum_{h \in \mathcal{Z}_x \cap \mathcal{Z}_y} z_h,$$

and further define $J_r = \mathrm{Re}(J) \in \mathbf{R}^{n \times n}$, as the entrywise real part of each entry of J. The matrix J is known as the loop impedance matrix, Desoer and Kuh (2010).

By letting $i(t) = (i_1(t), \ldots, i_n(t)) \in \mathbf{C}^n$, $u(t) = (u_1(t), \ldots, u_n(t)) \in \mathbf{C}^n$, for all $t \in \mathcal{T}$, it can be shown, that the total active power loss in the feeder is

$$i(t)^{\dagger} J_{\mathrm{r}} i(t) > 0. \quad (3)$$

To see this notice that the losses through each cable, may be written as

$$r_j(\sum_{\{k|j\in\mathcal{Z}_k\}} i_k(t))^\dagger(\sum_{\{k|j\in\mathcal{Z}_k\}} i_k(t)), \quad j=1,\ldots,m.$$

Summing for all cables, gives (3).

Additionally, the voltage at each household is

$$u(t) = u_s - Ji(t), \quad \forall t \in \mathcal{T}.$$

2.4 Voltage quality

The grid must be managed such that voltage variations throughout the radial are limited, *i.e.*, $u_{\min} \leq |u(t)| \leq u_{\max}$, where $|\cdot|$ denotes entry-wise complex magnitude, and $u_{\min}, u_{\max} \in \mathbf{R}$ are lower and upper bound on voltage magnitudes, respectively. This is equivalent to

$$u_{\min}^2 \leq |u(t)|^2 \leq u_{\max}^2, \quad \forall t \in \mathcal{T}. \tag{4}$$

The inequalities above are to be read element-wise.

2.5 Problem formulation

Given the model and constraints of both consumers and the grid, as well as the expression for grid losses presented above, we state the following main problem:

Problem 1. For given data:

- sets: $\mathcal{H}, \mathcal{H}_{\text{ev}}, \mathcal{H}_{\text{pv}}$,
- profiles: $\overline{p}_h(t)$, $\overline{p}_{\text{pv},h}(t)$, $\overline{q}_h(t)$ for each $h \in \mathcal{H}, t \in \mathcal{T}$,
- values: ψ_h, $t_{\text{ev},h}$ for each $h \in \mathcal{H}_{\text{ev}}$,
- matrices: J, J_r

solve

$$\begin{aligned} \underset{\tilde{p}_{\text{ev},h}(t),\, \tilde{q}_{\text{pv},h}(t)}{\text{minimize}} \quad & \sum_{t=1}^{T} i(t)^\dagger J_{\text{r}} i(t) \\ \text{subject to} \quad & u_{\min}^2 \leq |u(t)|^2 \leq u_{\max}^2, \\ & E_{\text{ev},h}(T) = E_{\text{dem},h}, \\ & E_{\min,h} \leq E_{\text{ev},h}(t) \leq E_{\max,h}, \\ & p_{\min,h} \leq \tilde{p}_{\text{ev},h}(t) \leq p_{\max,h} \\ & \tilde{q}_{\text{pv},k}(t) \leq \sqrt{s_{\max,k}^2 - \overline{p}_{\text{pv},k}^2(t)}, \\ & i_j(t) = f(p_j(t), q_j(t), u_j(t)), \end{aligned} \tag{5}$$

for all $t \in \mathcal{T}$, $j \in \mathcal{H}$, $h \in \mathcal{H}_{\text{ev}}$ and $k \in \mathcal{H}_{\text{pv}}$.

The practical interpretation of Problem 1 is to coordinate consumers such that losses are minimized, whilst obeying both grid constraints with respect to voltage variations, as well as consumer constraints, with respect to EV charging.

We remind the reader that the problem is stated in discrete time; hence in (5), $\tilde{p}_{\text{ev},h}(t), \tilde{q}_{\text{pv},h}(t)$ each represent a discrete variable for each $t \in \mathcal{T}$, and should not be confused with general time-domain functions.

In the next section, we elaborate on our approach for solving Problem 1, and formulate a benchmark strategy, which we use for comparison during numerical experiments.

3. OPTIMIZATION AND BENCHMARK

Our strategy is to identify the non-convex elements of Problem 1, in order to make convex approximations, and arrange a simplified problem, which we can solve globally, with known methods.

3.1 Optimization

Large parts of Problem 1 are convex, and requires no simplifications. For instance, the cost function can be shown to be convex in the real and imaginary parts of $i(t)$, respectively. The same applies for all EV and PV constraints. The only elements of (5) that are not convex, are the relation between power and current (2), and the voltage variation limits (4).

The voltage constraint (4) can be visualized as the annulus in Fig. 4, where the maximum allowed amplitude is in fact convex in the real and imaginary part, respectively. The lower limit is not a convex constraint. We approximate this by an affine constraint around a fixed operating point $\hat{u}(t) \in \mathbf{C}^n$, for each $t \in \mathcal{T}$:

$$\begin{aligned} u_{\min}^2 \leq |\hat{u}(t)|^2 &+ 2\text{Re}(\hat{u}(t))(\text{Re}(u(t)) - \text{Re}(\hat{u}(t))) \\ &+ 2\text{Im}(\hat{u}(t))(\text{Im}(u(t)) - \text{Im}(\hat{u}(t))). \end{aligned}$$

This simplification is illustrated graphically in Fig. 4.

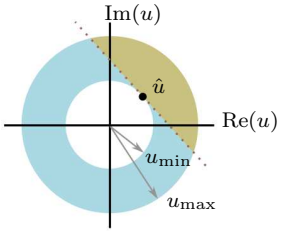

Fig. 4. Constraint for the voltage amplitude, where the annulus visualizes the allowed range of u. The dashed line illustrates a linear approximation for the lower limit, and the shaded region illustrates the resulting convexified constraint.

The consistency constraint (2), is non-convex on account of the division by $u_h^\dagger(t)$. We also replace this constraint by an affine approximation, around operating points $\hat{p}, \hat{q} \in \mathbf{R}^n$ and $\hat{u} \in \mathbf{C}^n$. We denote this affine approximation by $\hat{f}_{\hat{p},\hat{q},\hat{u}}$.

With these convexifications, Problem 1 can be approximated as:

Problem 2. Given:

- same information as in Problem 1,
- operating points $\hat{u}_h(t), \hat{p}_h(t), \hat{q}_h(t)$ for each $h \in \mathcal{H}$ and $t \in \mathcal{T}$

solve:

$$\begin{aligned} \underset{\tilde{p}_{\text{ev},h}(t),\, \tilde{q}_{\text{pv},h}(t)}{\text{minimize}} \quad & \sum_{t=1}^{T} i(t)^\dagger J_{\text{r}} i(t) \\ \text{subject to} \quad & \text{Re}(u(t))^2 + \text{Im}(u(t))^2 \leq u_{\max}^2, \\ & u_{\min}^2 \leq |\hat{u}(t)|^2 + 2\text{Re}(\hat{u}(t))(\text{Re}(u(t)) - \text{Re}(\hat{u}(t))) \\ & \quad +2\text{Im}(\hat{u}(t))(\text{Im}(u(t)) - \text{Im}(\hat{u}(t))) \\ & E_{\text{ev},h}(T) = E_{\text{dem},h}, \\ & E_{\min,h} \leq E_{\text{ev},h}(t) \leq E_{\max,h}, \\ & p_{\min,h} \leq \tilde{p}_{\text{ev},h}(t) \leq p_{\max,h} \\ & \tilde{q}_{\text{pv},k}(t) \leq \sqrt{s_{\max,k}^2 - \overline{p}_{\text{pv},k}^2(t)}, \\ & i_j(t) = \hat{f}_{\hat{p},\hat{q},\hat{u}}(p_j(t), q_j(t), u_j(t)), \end{aligned} \tag{6}$$

for all $t \in \mathcal{T}$, $j \in \mathcal{H}, h \in \mathcal{H}_{\text{ev}}$ and $k \in \mathcal{H}_{\text{pv}}$.

Problem 2 is convex and can be solved by known methods. Let the solution be denoted $i(t)^\star, q(t)^\star, p(t)^\star$, with

$$p(t)^\star = (p_1(t)^\star, \cdots, p_n(t)^\star), \quad q(t)^\star = (q_1(t)^\star, \cdots, q_n(t)^\star).$$

Since (6) was solved with an estimated voltage $\hat{u}(t)$, the true voltages resulting from the current $i(t)^\star$, may now be found through the post calculation

$$u_{\text{true}}(t) = u_{\text{s}} - Ji^\star(t), \quad \forall t \in \mathcal{T}.$$

Let $\hat{u}(t) = (\hat{u}_1(t), \cdots, \hat{u}_n(t))$. If

$$\|u_{\text{true}}(t) - \hat{u}(t)\| > \epsilon, \quad \forall t \in \mathcal{T},$$

for some tolerance $\epsilon > 0$, then the true voltage is far from the approximated voltage employed in the optimization. Our approach is then to update the voltage estimate, and re-solve Problem 2. This iterative approach can be formulated as:

Algorithm 1: Loss minimization procedure

(1) **Initialize** $\gamma > \epsilon > 0$ and $\hat{u}(t), \hat{p}(t), \hat{q}(t)$, for all $t \in \mathcal{T}$,

(2) **While** $\gamma > \epsilon$:
- Solve Problem 2 to obtain $i^\star(t), q^\star(t), p^\star(t)$, for all $t \in \mathcal{T}$
- set $\hat{p}(t) = p^\star(t)$ and $\hat{q}(t) = q^\star(t)$ for all $t \in \mathcal{T}$
- Calculate true voltage: $u_{\text{true}}(t) = u_{\text{s}} - J_{\text{z}} i^\star(t), \forall t \in \mathcal{T}$
- Set $\gamma = \|u_{\text{true}}(t) - \hat{u}(t)\|$,
- Set $\hat{u}(t) = u_{\text{true}}(t)$, for all $t \in \mathcal{T}$

(3) **Done**

If the iterative procedure converges such that $\|u_{\text{true}}(t) - \hat{u}(t)\| < \epsilon$, then $i^\star(t), q^\star(t), p^\star(t)$ are used as approximate solutions to the initial Problem 1.

This approach for finding an approximated solution to a non-convex problem, by solving a series of approximated, convex problems, is commonly known as sequential convex programming. Convergence properties for the algorithm above, were discussed by Dihn and Diehl (2010), for certain classes of non-convex problems. However, the method is in essence a heuristic, and general convergence and optimality guarantees are difficult to provide. The method has however been applied with great success within various fields, refer to *e.g.* Hovgaard et al. (2013) and Biegel et al. (2011).

3.2 Benchmark strategy

To illustrate the benefits of shifting the charge cycle of EVs, and utilizing reactive power control of the PVs, we present a benchmark strategy that does not utilize this flexibility. That is, the benchmark strategy charges each EV, when it is plugged in and does not utilize the PV capability to absorb or produce reactive power.

The benchmark strategy thereby enforces

$$\tilde{q}_{\text{pv},h}(t) = 0, \quad \forall h \in \mathcal{H}_{\text{pv}}, \quad t \in \mathcal{T},$$

and for all $h \in \mathcal{H}_{\text{ev}}$:

$$\tilde{p}_{\text{ev},h}(t) = \begin{cases} p_{\max,h}, & \text{if } t \geq t_{\text{ev},h} \text{ and } E_{\text{ev},h}(t) < E_{\text{dem},h} \\ 0, & \text{otherwise.} \end{cases}$$

From the topology of the grid, and impedances of each cable, the radial admittance matrix Y can be arranged Kundur (1993). Given Y, as well as $p_h(t), q_h(t)$ for each $h \in \mathcal{H}, t \in \mathcal{T}$, known methods exists for calculating the current and voltage of each consumer, *e.g.*, Gauss-Seidel and Newton-Raphson.

The following section describes in detail a test-case used as a foundation for numerical experiments in Section 5.

4. TEST-CASE

We consider a low-voltage distribution grid, of a residential neighborhood, located in Northern Jutland, Denmark. The entire low-voltage grid consists of three 10/0.4 kV transformer substations, with a total of 19 feeders and 316 residential consumers. We limit our attention to one of these feeders, servicing 34 residential consumers. The tree topology of the feeder, is illustrated in Fig. 5. Each consumer is modeled as described in Section 2.

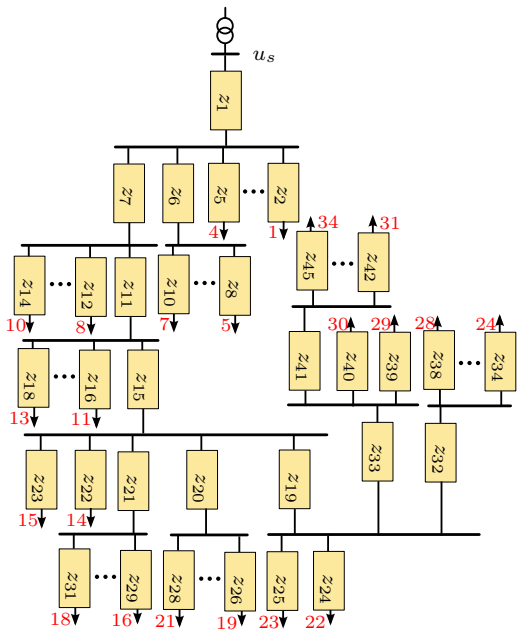

Fig. 5. Outline of the feeder employed for numerical experiments. Boxes are impedances and arrows indicate connection points of individual consumers. The numbers next to each arrow indicate the consumer numbering convention, to be used for classifying $\mathcal{H}, \mathcal{H}_{\text{ev}}, \mathcal{H}_{\text{pv}}$ in subsequent examples.

The resistive and reactive parameters of impedances, are presented in the following table. There are four different types of cables, as elaborated by Pillai et al. (2012):

Impedance nr.	**Res.** [Ω/m]	**Reac.** [Ω/m]
1, 7, 11	0.21	0.072
15, 19	0.32	0.075
6, 20, 21, 32, 33, 41	0.64	0.079
2-5, 8-10, 12-14, 16-18, 22-31, 34-40, 42-45	1.81	0.094

Provided the length of each cable in the feeder, combined with the data above, the impedances can be calculated. In the numerical experiments to follow, we consider a time-period of 21 hours, sampled in 10 minute intervals, starting at 14:00. The inflexible consumption of each consumer is modeled as known curves, presented in Fig. 6.

The data in Fig. 6 is retrieved from Nord Pool Spot (2013), and is representative of the daily consumption pattern of residential houses. With the curves in Fig. 6, the average daily energy consumption is 7.9 kWh. The inflexible consumption of all households are modeled with a constant power factor of 0.95.

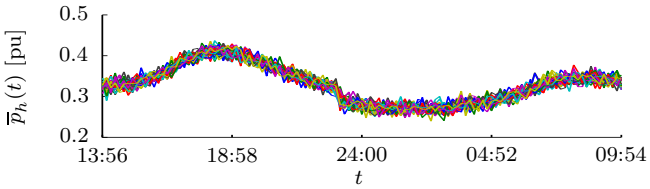

Fig. 6. The inflexible consumption of all households.

5. NUMERICAL EXPERIMENTS

In the following numerical experiments, we explore several different scenarios, related to the installation of EVs and PVs in the test-case. We examine the following scenarios:

1. Resilience of benchmark strategy against implementation of EVs and PVs separately.
2. Resilience of suggested coordination based strategy against implementation of EVs and PVs separately.
3. Benefit of coordination strategy over benchmark, with combined installations of EVs and PVs.

Scenario 1 substantiates the introductory example, and shows that by separately introducing EVs and PVs, unacceptable over- and under-voltages occur, if the inherent flexibility is not utilized. Scenario 2 shows that the voltage issues of Scenario 1 caused by EV consumption and PV production, can be alleviated by altering the EV charge profile, and utilizing PV reactive power. Finally, Scenario 3 shows that by combining the installation of EVs and PVs, all voltage issues can be alleviated by the proposed optimization strategy.

We employ pr-unit notation. The base voltage is set to 0.4 kV, and the base power is set to 1 kVA. All other quantities are transformed accordingly. The transformer phasor voltage is $u_s = 1\angle 0°$ pu. The Danish grid code requires that voltage variations are limited to $\pm 10\%$, however, following the example of Pillai et al. (2012), we shall employ $\pm 6\%$ as the constraint in our coordination, such as to leave sufficient margin for medium voltage grid variations. We refer to the 6% variation as a safety limit, and the 10% variation as the strict limit.

Fig. 7 presents the known generation of active power from households with solar panels. The active solar power output for all households is limited to 8 pu.

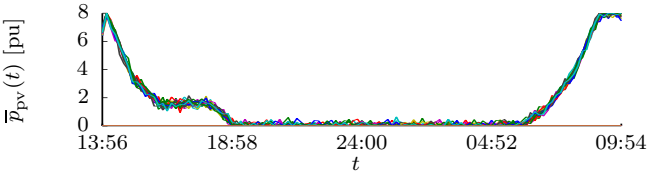

Fig. 7. The solar power, $\overline{p}_{\text{pv}}(t)$, based on data retrieved from the Danish Metrological Institute.

For all $h \in \mathcal{H}_{\text{ev}}$, we let $p_{\min} = -11$ pu, $p_{\max} = 11$ pu, $E_{\text{dem},h} = 25$ pu, and

$$t_{\text{ev},h} \in \mathcal{U}(14:00,\ 17:00), \quad E_{\text{ev},h}(t_{\text{ev},h}) \in \mathcal{U}(0,1),$$

where $\mathcal{U}(a,b)$ denotes a uniform distribution of $[a,b]$.

5.1 Resilience of benchmark strategy

We evaluate the effect of installing EVs and PVs in the grid, when the benchmark strategy is utilized. The voltage profile at the connection point for each consumer in Fig. 5, is obtained by Gauss-Seidel iterations. Scenario 1 and 2 above are simulated for the benchmark strategy, through the two configurations:

A. $\mathcal{H}_{\text{pv}} = \emptyset$ and $\mathcal{H}_{\text{ev}} = \{30, \ldots, 34\}$;
B. $\mathcal{H}_{\text{pv}} = \{1\text{-}7, 25\text{-}34\}$ and $\mathcal{H}_{\text{ev}} = \emptyset$.

The resulting voltage profiles from both configurations throughout the horizon, are presented in Fig. 8, with Configuration A illustrated in Fig. 8(top). Each curve shows the voltage over time in the connection point of a consumer. The step-like nature of the curves illustrates the time instances where each of the five EVs either start or finish charging, causing a voltage drop or increase, respectively.

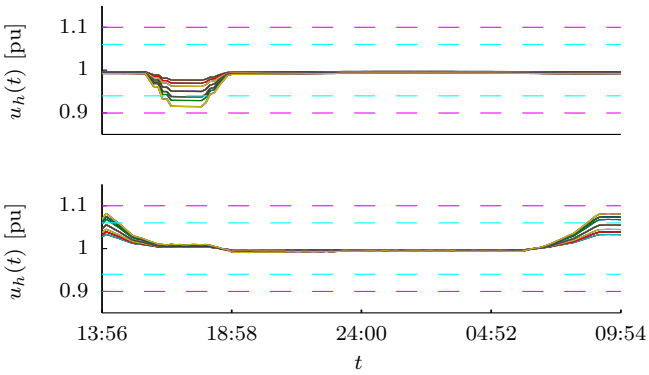

Fig. 8. **Top:** Voltage profile in the connection point of each consumer, resulting from benchmark strategy Configuration A (solid), and voltage variation limits (dashed). **Bottom:** Similarly, voltage profiles by Configuration B.

The voltage profiles violates the safety limit, and further, comes quite close to violating the strict limit, even though only five EVs are connected.

The experiment for Configuration B, results in the voltage profiles presented in Fig. 8(Bottom). Here, we see similar to Configuration A, that PVs introduce local over-voltages in the sense that the safety limit is violated in both the beginning and end of the simulation. Comparing these results, to the solar power presented in Fig. 7, it is clear that the time of the over-voltages coincide with the period of highest solar intensity. Since the solar power is not consumed locally, it is transported back to the medium voltage grid, which causes the over-voltages. For reference onwards, the maximum voltage experienced in Fig. 8(Bottom), is 1.081 pu.

5.2 Resilience of coordination based strategy

Employing the coordination strategy described previously, we perform again two numerical experiments for Scenario 1 and 2, with configurations

A. $\mathcal{H}_{\text{pv}} = \emptyset$ and $\mathcal{H}_{\text{ev}} = \mathcal{H}$,
B. $\mathcal{H}_{\text{pv}} = \{1\text{-}7, 25\text{-}34\}$ and $\mathcal{H}_{\text{ev}} = \emptyset$.

The reader should notice that now all households are installed with EVs, and not only the final five. The voltage profile obtained in Configuration A is illustrated in Fig. 9(Top). As evident, the coordination performed by the algorithm previously introduced, is able to support an EV for every household, without introducing under-voltages. The specific charge pattern for the EVs are

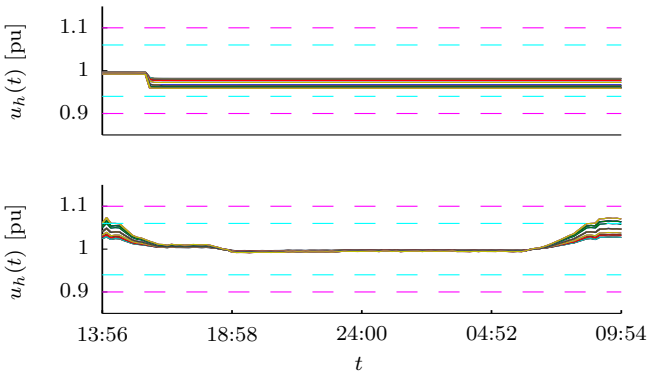

Fig. 9. **Top:** Voltage profile in the connection point of each consumer, resulting from optimization strategy Configuration A (solid), and allowed voltage range (dashed). **Bottom:** Similarly, voltage profiles by Configuration B.

shown in Fig. 10. Here, it is observed that all EVs are charged, roughly, with a constant power, in a way that averages out the load on the grid. Remember that the optimization minimizes losses, while obeying voltage constraints. Since losses are quadratic, averaging out the load of the grid reduces losses, compared to a faster charge schedule of the vehicles. From further numerical studies, this result appears to be reasonably consistent, also for other configurations of $\mathcal{H}_{\text{ev}}$.

In this work we have not included any price of electricity. Introducing for instance, a time-varying price signal would entail that both the cost of losses, as well as the cost of energy would vary across the horizon. Thereby, it is likely that less intuitive charge schedules would be prefferable. We shall leave this concern for future extensions.

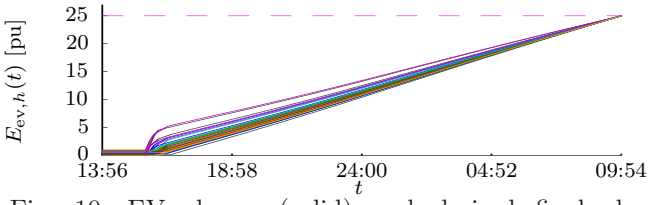

Fig. 10. EV charge (solid) and desired final charge (dashed), when employing optimization based approach.

For Configuration B above, the optimization based approach renders the voltage profiles presented in Fig. 9 (Bottom). We see that over-voltages are still present, however, the maximum voltage is now 1.073 pu, which is a reduction compared to the benchmark strategy, obtained solely through control of the reactive power for solar panels. There are two important comments related to the results in Fig. 9(Bottom):

- To avoid feasibility issues with the voltage profiles in the examples, we have reformulated the tight voltage constraints presented in Problem 1 and Problem 2, by soft constraints employing slack variables.
- We have over-dimensioned the solar panel inverters by 5 %, by letting $s_{\max} = 1.05 p_{\text{pv,max}}$, where $p_{\text{pv,max}}$ is the maximum active power output. This entails that when $\overline{p}_{\text{pv}}(t) = p_{\text{pv,max}}$, the constraint in (1) still allows the PV inverter to either produce or consumer some amount of reactive power. Introducing this over-dimensioning is what allows the optimization to improve the voltage. If no over-dimensioning was introduced, the optimization would not be able to improve voltage in periods where the active power output from the solar panels where saturated.

The table below illustrates the maximum voltage occurring in the grid for Configuration B above, for different levels of over-dimensioning of the solar panel inverters:

over-dimension [%]	0	5	10	20	30
voltage [pu]	1.081	1.073	1.070	1.064	1.060

Table 1. Reduction of over-voltages from various degrees of PV inverter over-dimensioning.

As illustrated by the table above, a sizeable overdimensioning of the PV inverter is required to fully remove the overvoltages. However, the following section illustrates how coordination between flexible consumption from EVs and local production from PVs can improve the voltage further. The benefit of over-dimensioning PV inverters was also discussed by Turitsyn et al. (2011).

5.3 Benefit of optimization strategy over benchmark

In this final experiment, we introduce EVs and PVs randomly throughout the feeder, such that the penetration of both PV and EV is around 50%. Employing both the benchmark and optimization based strategy, yields the results in Fig. 11, where Fig. 11(Top) and (Middle) presents the total power consumption, and the power consumption solely from EVs, respectively.

From the definition of the benchmark strategy, all EVs charge as soon as they are plugged in. This entails that there is a large peak in consumption in the beginning of the time-span of the simulation. Similarly, in the end of the simulation, when the solar power increase, there is a large negative consumption. This entails that the voltage profiles corresponding to the benchmark strategy, in Fig. 11(Bottom), initially show under-voltages when charging EVs, and later, over-voltages because the PV generated power is not absorbed.

Conversely, when using the optimization based strategy, the EV charging is postponed, and coordinated with the PV generation, such that consumption by EVs counteracts the production from PVs. Contrary to the benchmark strategy, this coordination entails that both over- and under-voltages are avoided.

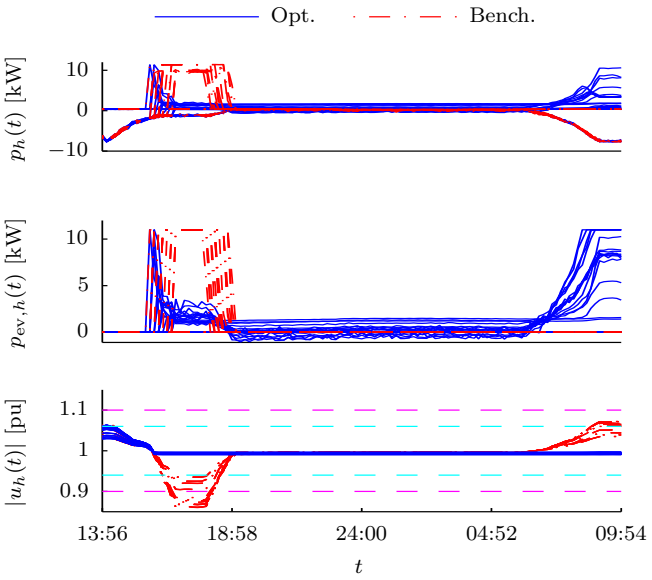

Fig. 11. Top: The total consumption in the optimized case (blue, solid), and the benchmark case (red, dashed). Middle: Corresponding EV charge schedule. Bottom: Resulting voltage profiles, as well as voltage limits (dashed, magenta).

In Fig. 11(Bottom), we see over-voltages in the very beginning of the simulation of both the benchmark and the optimized strategy. This is because at this time, there is some PV production, however, no EVs are available for charging. These over-voltages can thereby only be reduced by reactive power control of the solar panels. Pertaining to the previous discussion concerning over-dimensioning of converters, this example is conducted with 5 % inverter over-dimensioning. Even though the reactive power control reduces over-voltages, it is evident from the figure, that they are not completely removed. This illustrates an important point; that to avoid the potential over-voltages caused by PV generation, may require some flexible consumption in order to absorb the power of solar panels.

6. CONCLUDING REMARKS

This work has addressed future challenges of the electric distribution grid, emerging from expected changes in the nature of consumers. We have described how a future increase in the use of EVs and PVs may cause the grid to be overloaded, and unacceptable voltage variations to occur.

An optimization based strategy for employing flexibility of active and reactive power for EVs and PVs respectively, has been arranged. Using this strategy we have shown how coordination among individual EVs and PV facilities may be employed to reduce power losses in the grid, as well as alleviate issues pertaining to voltage variations, compared to a benchmark control strategy which does not utilize flexibility.

Numerical experiments, based on a true distribution grid located in Northern Jutland, Denmark, has illustrated how the posed optimization problem can assist in maintaining grid limitations, even when increasing the penetration of EVs and PVs far beyond the levels currently present in the Danish electric grid.

ACKNOWLEDGEMENTS

This work is supported in part by the Southern Danish Growth Forum and the European Regional Development Fund, under the project "Smart & Cool", and in part by the the Danish Council for Strategic Research (contract no 11-116843) within the 'Programme Sustainable Energy and Environment' under the project "EDGE" (Efficient Distribution of Green Energy).

REFERENCES

M. E. Baran and F. F. Wu. Network Reconfiguration in Distribution Systems for Loss Reduction and Load Balancing. *IEEE Transactions on Power Delivery*, 4 (2), 1989.

B. Biegel, M. Juelsgaard, M. Kraning, S. Boyd, and J. Stoustrup. Wind turbine pitch optimization. *IEEE Conference on Control Applications, Proceedings*, 2011.

Danish Energy Association and Energinet.dk. *Smart Grid i Danmark*. `www.danskenergi.dk`, 2010.

C. Desoer and E. Kuh. *Basic Circuit Theory*. McGraw-Hill, 2010.

Q. Dihn and M. Diehl. Local convergence of sequential convex programming for nonconvex optimization. *Recent Advances in Optimization and its Applications in Engineering*, pages 93–102, 2010.

Y. Guo, Y. Lin, and M. Sun. The impact of integrating distributed generations on the losses in the smart grid. *IEEE Power and Energy Society General Meeting*, 2011.

T. Hoff and D. Shugar. The value of grid-support photovoltaics in reducing distribution system losses. *IEEE Transactions on Energy Conversion*, 10(3):569–576, 1995.

T. Hovgaard, L. Larsen, S. Boyd, and J. Jørgensen. Mpc for wind power gradients - utilizing forecasts, rotor inertia, and central energy storage. *Proceedings of European Control Conference*, 2013.

International Energy Agency. *Technology Roadmap: Electric and plug-in hybrid electric vehicles*. `http://www.iea.org/`, 2011.

A. Ipakchi and F. Albuyeh. Grid of the future. *IEEE Power and Energy Magazine*, (april), 2009.

M. Juelsgaard, P. Andersen, and R. Wisniewski. Minimization of distribution grid losses by consumption coordination. *Proceedings of IEEE Multi-Conference on Systems and Control*, 2013.

P. Kundur. *Power system stability and control*. McGraw-Hill, 1993.

Nord Pool Spot. `http://www.nordpoolspot.com/`, 2013. Common Nordic Power Exchange.

J. Pillai, P Thøgersen, J. Møller, and B. Bak. Integration of electric vehicles in low voltage Danish distribution grids. *Power and Energy*, 2012.

K. Turitsyn, P. Sulc, S. Backhaus, and M. Chertkov. Options for Control of Reactive Power by Distributed Photovoltaic Generators. *Proceedings of the IEEE*, 99 (6):1063–1073, jun 2011.